miR-600 Acts as a Bimodal Switch that Regulates Breast Cancer Stem Cell Fate through WNT Signaling

Rita El Helou, Guillaume Pinna, Olivier Cabaud, Julien Wicinski, Ricky Bhajun, Laurent Guyon, Claire Rioualen, Pascal Finetti, Abigaelle Gros, Bernard Mari, et al.

Article

Cell Reports

miR-600 Acts as a Bimodal Switch that Regulates Breast Cancer Stem Cell Fate through WNT Signaling

Graphical Abstract

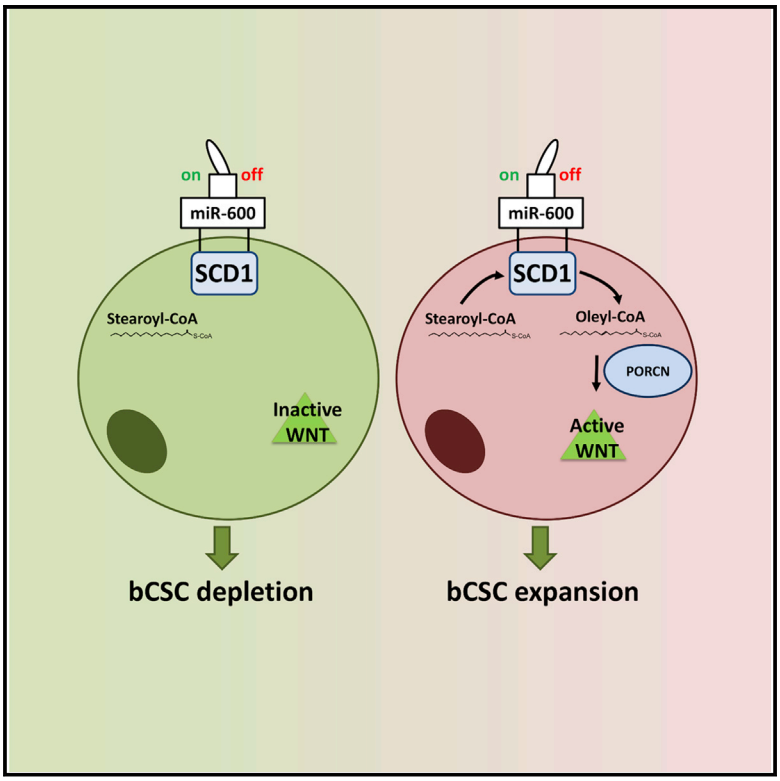

Authors

Rita El Helou, Guillaume Pinna, Olivier Cabaud, ..., Daniel Birnbaum, Emmanuelle Charafe-Jauffret, Christophe Ginestier

Correspondence

christophe.ginestier@inserm.fr

In Brief

El Helou et al. identify miRNAs that are able to balance bCSC fate. They find that miR-600 silencing results in bCSC expansion, while its overexpression reduces bCSC self-renewal. miR-600 was further found to regulate WNT signaling through SCD1, and miR-600 expression correlates with clinical outcome.

Highlights

- miR-600 expression balances self-renewal and differentiation of bCSCs
- miR-600 acts as a regulator of WNT signaling through SCD1 modulation
- Low miR-600 expression in breast tumors is associated with poor prognosis

Accession Numbers

E-MTAB-5393

El Helou et al., 2017, Cell Reports *18*, 2256–2268
February 28, 2017
http://dx.doi.org/10.1016/j.celrep.2017.02.016

OPEN ACCESS
CellPress

Cell Reports
Article

miR-600 Acts as a Bimodal Switch that Regulates Breast Cancer Stem Cell Fate through WNT Signaling

Rita El Helou,[1] Guillaume Pinna,[2,3] Olivier Cabaud,[1] Julien Wicinski,[1] Ricky Bhajun,[4,5,6] Laurent Guyon,[4,5,6] Claire Rioualen,[7] Pascal Finetti,[1] Abigaelle Gros,[1] Bernard Mari,[8,9] Pascal Barbry,[8,9] Francois Bertucci,[1] Ghislain Bidaut,[7] Annick Harel-Bellan,[2,3] Daniel Birnbaum,[1] Emmanuelle Charafe-Jauffret,[1] and Christophe Ginestier[1,10,*]

[1]Molecular Oncology "Equipe labellisée Ligue Contre le Cancer," Aix-Marseille Université, CNRS, INSERM, Institut Paoli-Calmettes, CRCM, 13273 Marseille, France
[2]Plateforme ARN interférence (PARi), Service de Biologie Intégrative et de Génétique Moléculaire, I2BC, UMR 9198, CEA Saclay, 91191 Gif-sur-Yvette, France
[3]Université Paris-Sud, Gif-sur-Yvette, 91400 Orsay, France
[4]Université Grenoble-Alpes, 38000 Grenoble, France
[5]CEA, iRTSV, Biologie à Grande Echelle, 38054 Grenoble, France
[6]INSERM, U1038, 38054 Grenoble, France
[7]Plateform Integrative Bioinformatics, Aix-Marseille Université, CNRS, INSERM, Institut Paoli-Calmettes, CRCM, Cibi, 13273 Marseille, France
[8]CNRS, Institute of Molecular and Cellular Pharmacology, Sophia Antipolis, 06560 Valbonne, France
[9]University of Nice Sophia Antipolis, 06000 Nice, France
[10]Lead Contact
*Correspondence: christophe.ginestier@inserm.fr
http://dx.doi.org/10.1016/j.celrep.2017.02.016

SUMMARY

Breast cancer stem cells (bCSCs) have been implicated in tumor progression and therapeutic resistance; however, the molecular mechanisms that define this state are unclear. We have performed two microRNA (miRNA) gain- and loss-of-function screens to identify miRNAs that regulate the choice between bCSC self-renewal and differentiation. We find that micro-RNA (miR)-600 silencing results in bCSC expansion, while its overexpression reduces bCSC self-renewal, leading to decreased in vivo tumorigenicity. miR-600 targets stearoyl desaturase 1 (SCD1), an enzyme required to produce active, lipid-modified WNT proteins. In the absence of miR-600, WNT signaling is active and promotes self-renewal, whereas overexpression of miR-600 inhibits the production of active WNT and promotes bCSC differentiation. In a series of 120 breast tumors, we found that a low level of miR-600 is correlated with active WNT signaling and a poor prognosis. These findings highlight a miR-600-centered signaling network that governs bCSC-fate decisions and influences tumor progression.

INTRODUCTION

Tumor heterogeneity contributes to therapy failure and disease progression. The origin of this heterogeneity is explained by both the coexistence of clones with various mutational events and a hierarchical organization where several subpopulations of self-renewing cancer stem cells (CSCs) maintain the long-term oligoclonal nature of the neoplasm (Kreso and Dick, 2014). CSCs drive tumor growth, can be resistant to conventional therapies, and initiate metastasis development (Visvader and Lindeman, 2012). Thus, developing CSC-targeting therapies is of major interest and requires insight into the unique molecular circuitry of CSCs compared to non-CSCs (Liu and Wicha, 2010). The cardinal property of a CSC is its self-renewal program. Deciphering molecular mechanisms regulating self-renewal and differentiation in proliferating CSCs is a key step in the development of new therapeutic strategies. MicroRNAs (miRNAs), a class of small non-coding RNAs that regulate gene expression at the post-transcriptional level, have been proposed to be key players of the complex regulatory circuit controlling CSC fate. Several miRNAs are either highly expressed or excluded from the CSC compartment (Liu et al., 2012a; Garofalo and Croce, 2015). miRNAs regulate gene expression by base-pairing to the 3′ UTRs of target mRNAs, inducing mRNA degradation and/or translational inhibition (Djuranovic et al., 2011). Let-7 and microRNA (miR)-200 families were among the first miRNAs described to regulate the CSC self-renewal program (Yu et al., 2007; Shimono et al., 2009). Several studies have implicated miRNAs as central regulators of CSC self-renewal in multiple tumor types, including leukemia (Song et al., 2013), colon cancer (Bu et al., 2013; Hwang et al., 2014), prostate cancer (Liu et al., 2011), hepatocellular carcinoma (Ma et al., 2010), brain tumors (Wang et al., 2014), and breast cancer (Polytarchou et al., 2012; Liu et al., 2012b; Cai et al., 2013; Taube et al., 2013).

Given the central role of CSCs in tumor growth and of miRNAs in CSC biology, it is crucial to perform a comprehensive elucidation of the regulators that specify CSC identity. Here, we have studied breast CSCs (bCSCs) and performed two concurrent human miRNA gain- and loss-of-function screens using pre-miRs

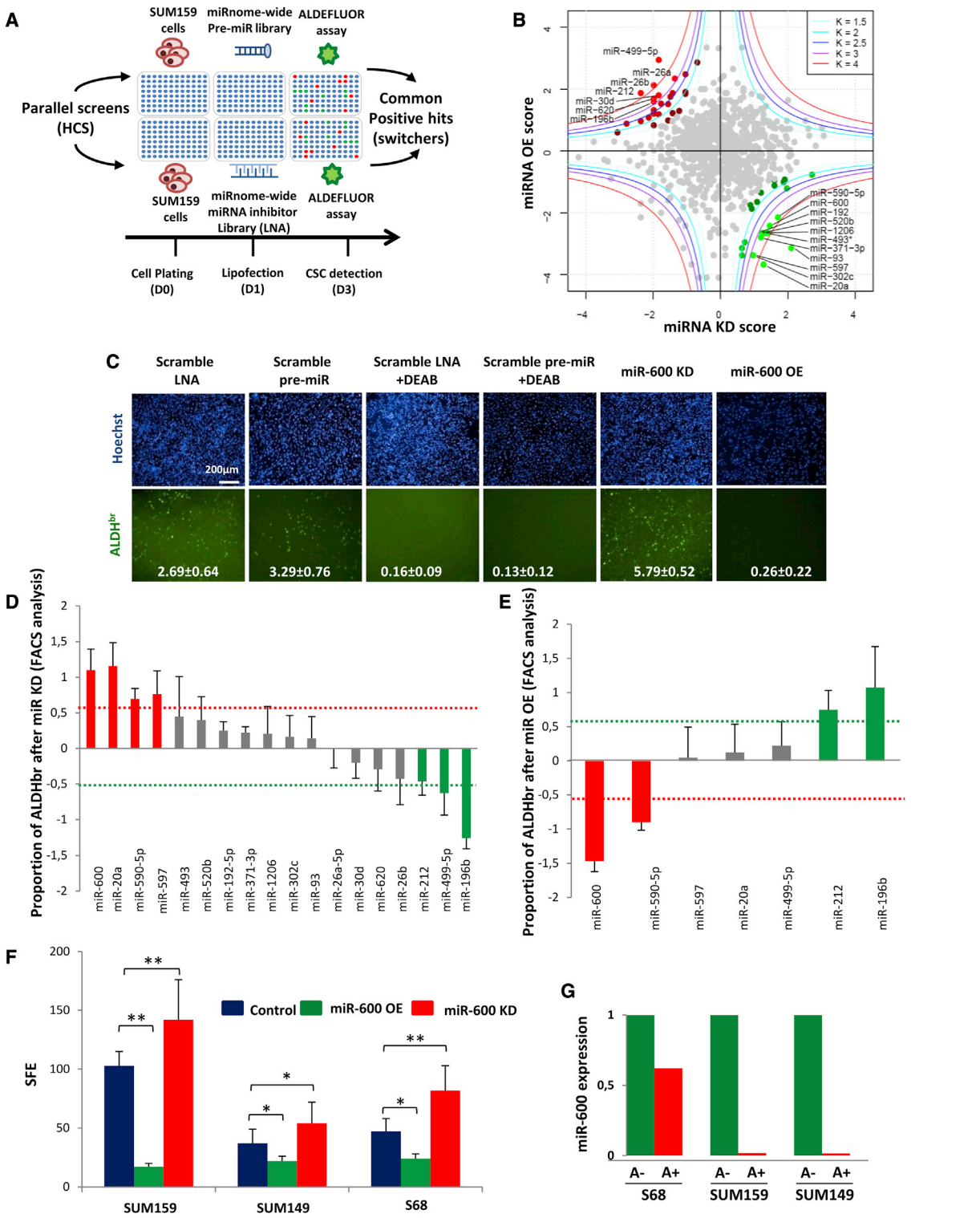

Figure 1. Parallel miRNA-Based Genetic Screens Identify miRNA Bimodal Switchers that Regulate bCSC Fate

(A) Workflow of the miRNome-wide miRNA OE and KD screens. miRNAs that could oppositely influence the bCSC/non-CSC ratio when overexpressed (OE) and knocked down (KD) (switchers) were considered as candidates.

(B) Bi-dimensional plot of the two concurrent screens (x axis, miRNA KD z-score; y axis miRNA OE *Z* score). Results are expressed according to a composite score (see Supplemental Experimental Procedures). Each green dot represents a miRNA that favors CSC depletion when overexpressed and CSC expansion

(legend continued on next page)

as miRNAs mimics and locked nucleic acid (LNA)-modified probes as inhibitors. These functional screens identify miRNAs that influence bCSC-fate decision. Focusing on miR-600, we have shown that overexpression of this miRNA regulates WNT signaling by suppressing the expression of stearoyl desaturase 1 (SCD1), an enzyme required to produce active, lipid-modified WNT proteins. We find that miR-600 expression regulates the bCSC subpopulation in vivo and that its expression level correlates with overall survival in breast cancer patients.

RESULTS

miRNome-wide Parallel Screens Identify Bimodal Switcher miRNAs that Regulate bCSC Fate

We previously demonstrated that the brightest cell subpopulations of breast cancer cell lines (BCLs) stained with ALDEFLUOR, a reporter probe of cellular ALDH enzymatic activity, are strongly enriched in CSCs (Charafe-Jauffret et al., 2009; Ginestier et al., 2007). To identify miRNAs that may regulate bCSC fate, we studied the effects of miRNA modulation in a miniaturized ALDEFLUOR-probed CSC detection assay. Systematic and unbiased miRNA modulation was achieved by performing two concurrent miRNome-wide loss- and gain-of-function screens in the SUM159 BCL cell line using LNA and pre-miR libraries as miRNA inhibitors and mimics, respectively (Figure 1A). After 72 hr of miRNA modulation, plates were imaged by means of a high-content epifluorescence microscope, and individual cells were detected using an automated image-segmentation algorithm (see Experimental Procedures). To identify miRNAs that could influence the bCSC/non-CSC ratio, we first normalized the variation of the CSC proportion upon overexpression (OE) or knockdown (KD) of a given miRNA with the CSC proportion detected in the negative controls (SUM159 cells transfected with a scrambled LNA or a scrambled pre-miR) (Table S1). For each miRNA, the variation (fold change) of the CSC/non-CSC ratio upon miRNA OE was plotted according to the variation of the CSC/non-CSC ratio upon miRNA KD (Figure 1B). We developed a composite score (see Experimental Procedures) to select miRNAs acting as bimodal switchers of CSC equilibrium and ended up identifying 18 miRNAs as top candidates ($K \geq 3$). Overexpression of seven of these miRNAs (miR-26a, miR-26b, miR-30d, miR-196b, miR-212, miR-499-5p, and miR-620) resulted in CSC expansion, whereas overexpression of the eleven others (miR-20a, miR-93, miR-192, miR-302c, miR-371-3p, miR-493*, miR-520b, miR-590-5p, miR-597, miR-600, and miR-1206) induced CSC depletion. Utilizing a network-based approach (Bhajun et al., 2015; Shannon et al., 2003), we connected the 18 candidate miRNAs based on their common predicted targets and identified miRNA hit groups (Figure S2). The most relevant group contained members of the miR-17/92 cluster and its paralogs. Supporting our results, different members of this cluster are known to downregulate the CSC population and balance CSC fate by inducing cell differentiation (Liu et al., 2012b; Cioffi et al., 2015; Srivastava et al., 2015).

Next, we generated a focused library comprising all candidate miRNAs selected from the primary screens, and we performed validation experiments using flow cytometry analysis. The miRNA KD results from the primary screens were confirmed for 7 out of 18 candidates (Figure 1D). A bimodal switcher effect in miRNA OE conditions was confirmed for four of these seven miRNAs (miR-600, miR-590-5p, miR-212, and miR-196b; Figure 1E). To extend these observations, we tested the effect of miRNA OE or KD for these four hits in two additional BCLs (SUM149 and S68). We first confirmed that each of these four miRNAs was expressed in our three BCLs (Figure S3). After modulation of miRNAs expression, only miR-600 OE or KD showed a reproducible switcher effect in all the BCLs (Figure S3). The effect of miR-600 modulation on the bCSC population was accompanied by moderate effect on cell proliferation after OE 600 and no apoptosis induction (Figure S3). We next performed a functional in vitro assay based on tumorsphere formation to validate the functional effect of miR-600 OE and KD on the CSC population. Following miR-600 OE, depletion of the CSC population was associated with a decrease in tumorsphere-forming efficiency (SFE), while miR-600 KD expanded the number of tumorspheres formed in all three tested BCLs (Figure 1F). Importantly, miR-600 expression level, as measured by qRT-PCR, was lower in CSC populations than in non-CSC populations (Figure 1G). Taken together, these data suggest that miR-600 acts as a bimodal regulator of bCSC fate.

miR-600 Modulation Balances the bCSC Pool In Vivo

In vivo xenotransplantation remains the gold standard to prove that the balance between bCSC self-renewal and differentiation is affected. To show that miR-600 overexpression affects the CSC self-renewal/differentiation balance in vivo, we infected single-cell suspensions, isolated from established patient-derived xenograft (PDX) models (Charafe-Jauffret et al., 2013), with lentiviral vectors (lenti-miR-600, lenti-sponge 600, and lenti-CTRL) to generate stable miR-600 OE, miR-600 KD, and control PDX models. 3 days post-transduction, infected cells were sorted based on their DsRed positivity and then xenografted in recipient mice using limiting-dilution transplantation assay (Figure 2A). In two independent PDX models (CRCM168x and CRCM494x), tumor cells overexpressing miR-600 had markedly reduced tumor-initiating capacity in recipient mice compared to control, whereas

when downregulated (and vice versa for the red dots). 18 candidate miRNAs with bimodal switcher activity were selected according to a score selection threshold $K \geq 3$. Hyperboles are lines of same composite scores (iso-score lines).

(C) Representative images of the high-content screening (HCS) captures. Hoechst nuclear DNA staining is shown in blue and ALDEFLUOR cellular staining in green.

(D and E) Validation of candidate miRNAs using FACS analysis. CSC/non-CSC ratios are represented after KD (D) or OE (E) of the candidate miRNAs. Those with a $|\log2\ (\text{CSC/non/CSC ratio})| \geq 0.5$ were considered as validated hits.

(F) Tumorsphere-forming efficiency (SFE) after miR-600 KD or OE. The relative number of tumorspheres formed in each condition is represented in a bar plot for three different breast cancer cell lines (SUM159, SUM149, and S68) ($n = 5$, $^*p < 0.05$, $^{**}p < 0.01$).

(G) Relative expression levels of miR-600 measured by qRT-PCR in $ALDH^{br}$ (A+) and $ALDH^{low}$ (A−) cell populations from three different breast cancer cell lines (S68, SUM159, and SUM149). Results are expressed as mean ± SD.

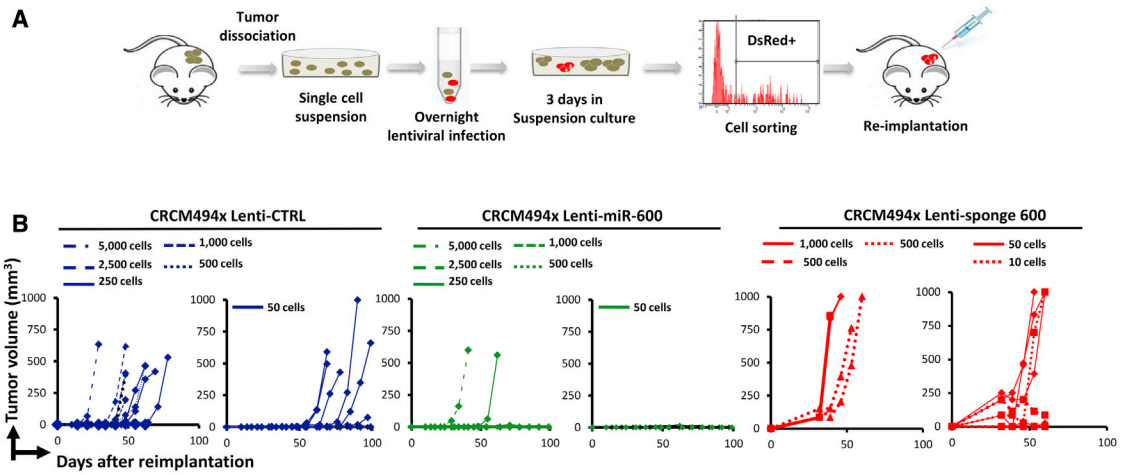

C

	Limiting Dilution Assay (number of injected cells)							
	10	50	250	500	1,000	2,500	5,000	10,000
CRCM494x Lenti-CTRL (outgrowth/injected fatpads)	0/2	5/12	4/6	3/4	4/4	3/3	1/1	
CRCM494x Lenti-miR600 (outgrowth/injected fatpads)	0/2	0/8	1/4	0/2	0/2	0/1	1/1	
CRCM494x Lenti-sponge 600 (outgrowth/injected fatpads)	1/4	3/4	2/2	1/1	1/1			
CRCM168x Lenti-CTRL (outgrowth/injected fatpads)				1/5	1/4	2/4	1/2	1/3
CRCM168x Lenti-miR600 (outgrowth/injected fatpads)				0/3	0/1	0/6		0/2
CRCM168x Lenti-sponge 600 (outgrowth/injected fatpads)				1/2	1/2	1/1	3/3	

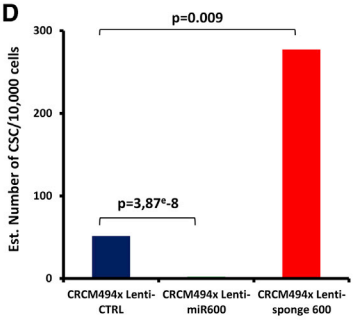

Figure 2. miR-600 Modulation Balances CSC Frequency In Vivo

(A) Workflow of the experimental protocol used for the lentiviral infection of cells from patient-derived xenografts (PDXs).

(B) FACS-sorted DsRed-positive cells were implanted using a limiting dilution assay in the fat-pads of NOD/SCID mice. Tumor growth kinetics are represented for CRCM494x PDX infected with Lenti-CTRL, Lenti-miR-600, or Lenti-sponge 600 (one tumor growth curve per injected fat-pad).

(C) Table showing the number of outgrowths generated in NOD/SCID mouse fat pads as a function of the amount of injected cells isolated from CRCM494x (or CRCM168x) Lenti-CTRL, Lenti-miR-600, or Lenti-sponge 600.

(D) bCSC frequency was calculated using an extreme limiting dilution analysis (ELDA) algorithm. Results are expressed as the estimated number of CSCs for 10,000 tumor cells.

it increased upon miR-600 KD (Figures 2B and S4). As determined by limiting dilution analysis (LDA), in vivo bCSC frequency was lower in the miR-600 OE tumor cell population (CRCM494x Lenti-miR-600 OE, 1:4,416, confidence interval [CI], 1,090–17,890; CRCM168x Lenti-miR-600 OE, 1:inf. (infinity), CI, inf.–12,518) than in the control cell population (CRCM494x Lenti-CTRL, 1:192, CI, 101–365; CRCM168x Lenti-CTRL, 1:7,370, CI, 3,024–17,966) (CRCM494x p = 3.87e-8; CRCM168x p = 0.0068). Conversely, we observed a greater bCSC frequency in the miR-600 KD tumor cell population (CRCM494x Lenti-sponge 600, 1:36, CI, 13–100; CRCM168x Lenti-CTRL, 1:940, CI, 301–2,943) (CRCM494x p = 0.009; CRCM168x p < 0.004) (Figures 2C, 2D, and S4). These in vivo observations confirm our in vitro results and strengthen the role of miR-600 as a key player in bCSC fate.

Identification of SCD1 as a Downstream Target of miR-600

To identify the mechanism(s) whereby miR-600 exerts its biological effect on bCSC, we established the gene expression profiles of fluorescence-activated cell sorting (FACS)-sorted SUM159 $ALDH^{br}$ cells transiently transfected with either miR-600 OE vector or its corresponding control vector (Figure 3A). We observed an overrepresentation of miR-600 predicted target genes (ArrayExpress: E-MTAB-5393 and TargetScan database; Garcia et al., 2011) among the genes downregulated after miR-600 OE (p value < 0.01; false discovery rate [FDR] < 0.25) (Figure 3B; Table S2). Because target gene prediction of miRNAs is challenging due to mismatch tolerance in miRNA-target mRNA complementarity, we used MiRonTop algorithm to integrate our gene expression profiles with miRNA target prediction datasets into a single meta-analysis (Le Brigand et al., 2010). This algorithm selects significantly downregulated transcripts following the overexpression of a specific miRNA and generates enrichment scores according to the spatial distribution of predicted miRNA target sites along the selected transcripts. MiRonTop analysis validated the enrichment of miR-600 predicted targets in the population of downregulated transcripts (Figure 3C).

We focused our next set of experiments on a subset of 19 transcripts with the highest enrichment score (log2 fold change <−0.7; p value < 0.01) (Table S3). To functionally validate these

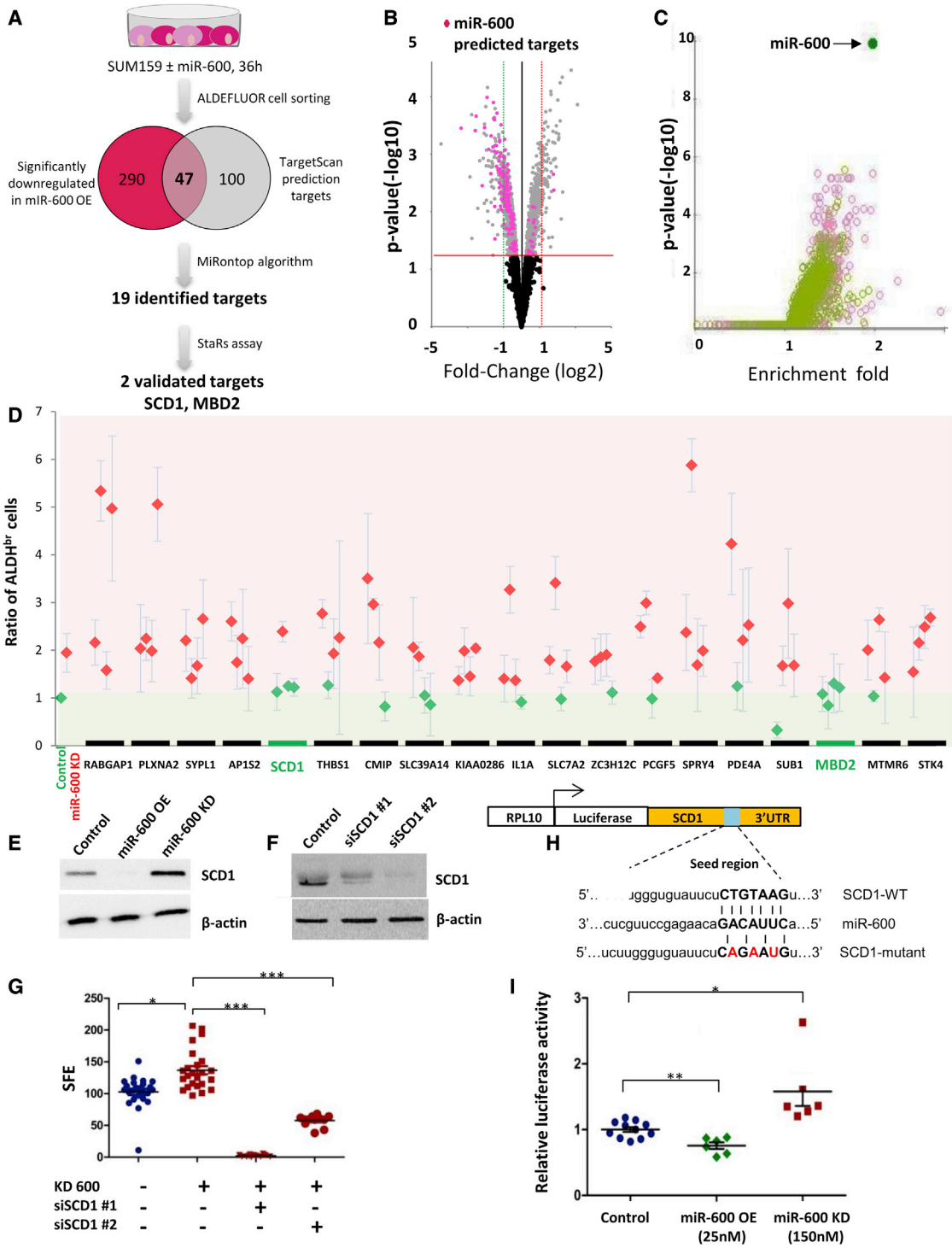

Figure 3. Identification of miR-600 Functional Target Genes

(A) Schematic representation of the experimental design to identify miR-600 functional target genes.

(B) Volcano plot of the gene expression profiling results. Scatter points represent genes, the x axis is the log2 fold change of the gene expression ratio between ALDH^{br} miR-600 OE treated versus untreated cells, and the y axis is the probability that a gene has statistical significance in its differential expression (genes with a FDR > 0.25 are highlighted as black dots). miR-600 predicted target genes from TargetScan database are highlighted as red dots.

(C) Graph derived from MiRonTop bioinformatics tool showing the overrepresentation of miR-600 seed complementary sequences in the 3′ UTR of down-regulated transcripts. Representation of TargetScan predicted targets in the set of downregulated genes was compared with the set of all expressed genes. For

(legend continued on next page)

19 transcripts as miR-600 targets, we performed a STarS (suppressor target screen) assay (Polesskaya et al., 2013), an unbiased screening approach to identify miR-600 functional targets. The STarS assay relies on the screening of a focused small interfering RNA (siRNA) library targeting the 19 MiRonTop selected transcripts, each siRNA being systematically and individually co-transfected with miR-600 LNA. The genes targeted by the siRNAs able to ''rescue'' the CSC expansion induced by miR-600 KD define a list of functional targets of miR-600 in the context of CSC equilibrium regulation. We designed a focused library of 76 siRNAs targeting our 19 candidates (4 siRNAs per candidate), and we set up a STarS assay to test each of the 76 siRNAs individually combined with miR-600 LNA. We selected siRNA/miR-600 LNA combinations able to restore the normal CSC ratio as measured in the control conditions (scrambled siRNA/scrambled LNA). Among the 19 candidate genes tested, only *SCD1* and *MBD2* silencing in miR-600 KD conditions restored the normal CSC ratio for at least three out of the four tested siRNA sequences (Figure 3D). Collectively, these data suggest that *SCD1* and *MBD2* serve as functional targets of miR-600 in bCSCs.

MBD2 is part of the methyl-CpG-binding domain family of protein that contributes to establishment and/or maintenance of transcriptional repression by recruiting enzymes that locally modify histones (Wood and Zhou, 2016). SCD1 is an enzyme of the fatty acid metabolism that generates mono-unsaturated fatty acids (MUFAs) from saturated fatty acid precursors, such as palmitoyl-coenzyme A and stearoyl-coenzyme A. SCD1 is required to produce active, lipid-modified WNT proteins (Rios-Esteves and Resh, 2013). Only lipid-modified WNT proteins can be secreted to activate the canonical WNT pathway, which is implicated in cell fate determination during development and oncogenesis in adult tissues (Ring et al., 2014). Based on the key role of WNT signaling in bCSC fate (Korkaya et al., 2009), we focused our study on *SCD1* as an miR-600 target. We first confirmed that endogenous SCD1 protein expression was regulated by miR-600 (Figure 3E) and that transient *SCD1* inhibition with two potent siRNAs (Figure 3F) was able to suppress the miR-600 KD effect on SUM159 CSCs using a tumorsphere-formation assay (Figure 3G). This result was also confirmed in SUM149 cells (Figure S5). SCD1 silencing had a limited effect on cell proliferation and reduced bCSC population in an apoptosis-independent manner (Figure S5), suggesting a role in bCSC-fate decisions. To further evaluate miR-600's direct regulation of *SCD1*, we developed a reporter assay using two plasmids with luciferase expression under the control of *SCD1* 3′ UTR. One plasmid had the *SCD1* 3′ UTR wild-type sequence (SCD1-WT), while the other had the *SCD1* 3′ UTR with mutations in the seed sequence of the miR-600 site (SCD1 mutant) (Figure 3H). Relative luciferase activity of the SCD1-WT construct (normalized to the luciferase activity of SCD1 mutant) was lower in cells treated with miR-600 OE and higher in cells treated with miR-600 KD (Figure 3I). Altogether, these results strongly suggest that miR-600 may regulate CSC-fate decisions in breast cancer cells by directly controlling *SCD1* expression.

miR-600 Controls bCSC Fate by Regulating WNT/β-Catenin Signaling through SCD1

Because SCD1 controls WNT secretion, we examined whether miR-600 could control bCSC fate through a miR-600/SCD1/WNT axis. We first confirmed that SCD1 regulates WNT/β-catenin signaling in our BCL models using a β-catenin bioluminescent reporter assay (TOPflash normalized with FOPflash). As expected, *SCD1* inhibition decreased the transactivating activity of β-catenin (Figure 4A). Moreover, analysis of a transcriptomics *SCD1* KD experiment using gene set enrichment analysis (GSEA) confirmed that *SCD1* inhibition resulted in a downregulation of WNT target genes (Figure S5). Additionally, *SCD1* inhibition resulted in a decrease of β-catenin relocation to the nucleus (Figure 4B; quantification in Figure S5). Because nuclear translocation and activation of β-catenin are rendered possible by the phosphorylation and inactivation of GSK3-β, we measured the level of GSK3-β phosphorylation in conditions where *SCD1* is inhibited (Figures 4C and S5). As expected, we observed a decrease of phosphorylated GSK3-β, supporting that, in our cellular models, SCD1 controls the WNT signaling pathway.

SCD1 generates oleic acid (OA), a MUFA transferred to the WNT protein via Porcupine/PORCN (Rios-Esteves and Resh, 2013), a membrane-bound O-acyltransferase that palmitoleates the WNT factors. To further validate the role of SCD1 in the control of WNT signaling pathway, we evaluated whether exogenous OA addition to the culture medium was able to rescue *SCD1* inhibition. Exogenous OA in the culture medium restored the $ALDH^{br}$ cells after *SCD1* inhibition (Figure 4D). It also partially restored the tumorsphere-formation efficiency (Figure 4E) and reactivated the transactivating activity of β-catenin (Figure 4F). These results show that, in our cellular models, SCD1 controls the WNT signaling pathway.

We then evaluated the role of miR-600 in WNT/β-catenin signaling. miR-600 OE resulted in a decrease in β-catenin transactivator activity, nuclear β-catenin, phosphorylated GSK3-β, and WNT3A ligand secretion (Figures 4G–4J; quantification in

each miRNA, a fold enrichment value (horizontal axis) and an associated p value (vertical axis) were calculated. The best enrichment score and p value was obtained for miR-600.

(D) Representation of the STarS assay results. A focused library of 76 siRNAs targeting 19 putative miR-600 target genes (4 siRNAs per gene) was designed and assayed for CSC/non-CSC ratio modulation in miR-600 KD SUM159 cell line. Green dots represent siRNAs that significantly rescue the CSC proportion increase induced by miR-600 KD, whereas red dots represent siRNAs unable to restore control CSC/non-CSC ratio. A gene was considered as a functional target of miR-600 when at least three out of four siRNAs restored the initial CSC ratio (i.e., *SCD1* and *MBD2*).

(E) SCD1 protein expression level after miR-600 modulation evaluated by western blot. β-Actin was used as a loading control.

(F) *SCD1* siRNA KD efficiency was evaluated by western blot. β-Actin was used as a loading control.

(G) Tumorsphere-forming efficiency (SFE) after miR600 KD and *SCD1* inhibition. The amount of formed tumorspheres is represented for each condition.

(H) Schematic of miR-600 putative target sites in the *SCD1*-3′ UTR. The mutated sites of the *SCD1* mutant construct are highlighted in red.

(I) Luciferase assay of SCD1-WT and mutant constructs after miR-600 OE or miR-600 KD. Results are expressed as mean ± SD (*$p < 0.05$; **$p < 0.01$; ***$p < 0.001$).

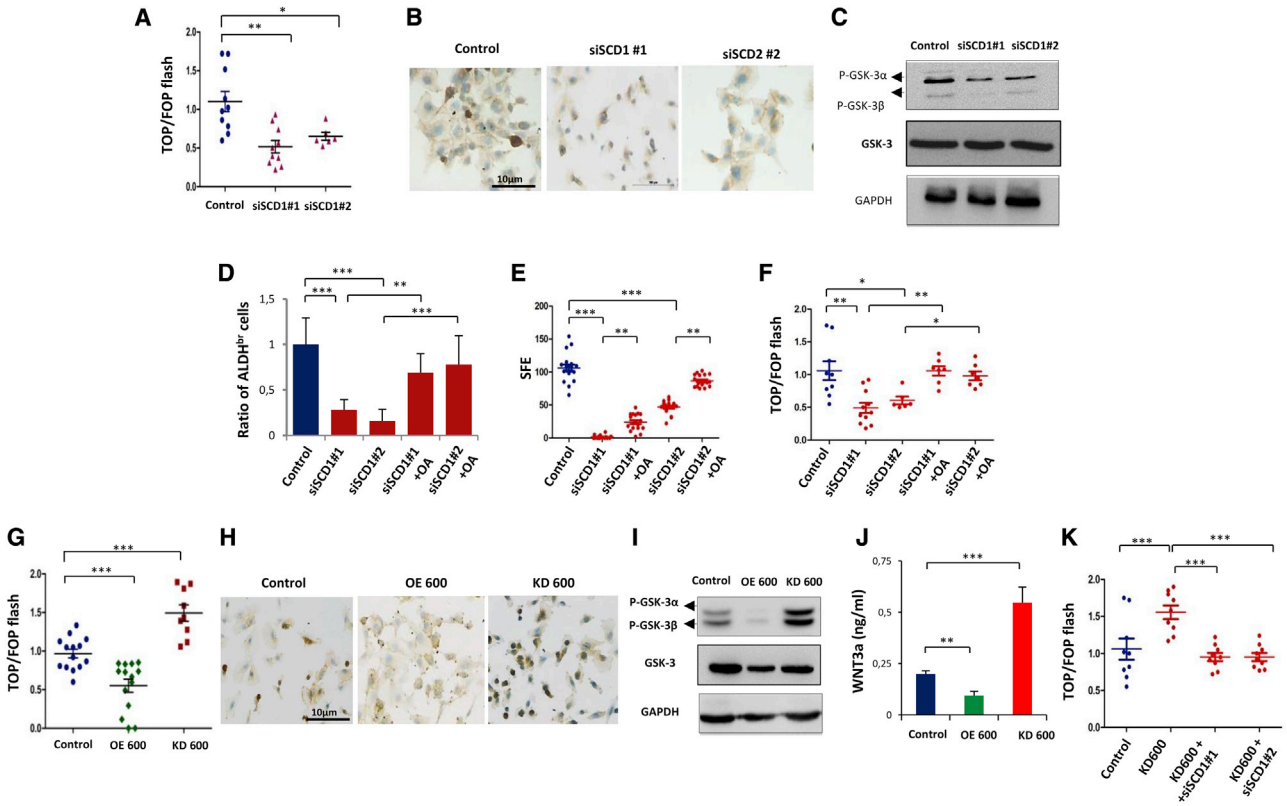

Figure 4. miR-600/SCD1 Axis Targets the WNT Signaling Pathway in bCSCs

(A–C) Effect of *SCD1* KD on WNT signaling pathway. *SCD1* KD was achieved using two different siRNAs (siSCD1#1 and #2). (A) WNT signaling activity measured by TOPflash assay normalized with FOP activity. (B) Immunostaining of β-catenin in SUM159 cells. β-catenin localization is shown in brown. (C) Phosphorylated GSK3-β expression measured by western blotting. Total GSK3-β and GAPDH expression were used as controls.

(D–F) Evaluation of compensatory effects of oleic acid (OA) supplementation after *SCD1* KD. (D) Evolution of the relative proportion of $ALDH^{br}$ cells after OA supplementation. (E and F) Bee swarm plots of the number of tumorspheres formed (SFE) and β-catenin transactivation after OA supplementation.

(G–I) Effect of miR-600 OE and KD on WNT signaling pathway was evaluated as described in (A)–(C).

(J) Level of soluble WNT3A in the medium measured by ELISA assay after miR-600 modulation.

(K) Evaluation of WNT signaling activity in cells double KD for SCD1 and miR-600 is represented by a bee swarm plot of β-catenin transactivation level (TOPflash). In bee swarm plots, a dot corresponds to an individual experiment. Results are expressed as mean ± SD (*$p < 0.05$; **$p < 0.01$; ***$p < 0.001$).

Figure S6). Conversely, miR-600 KD induced a strong increase in β-catenin transactivator activity, an accumulation of β-catenin in the nucleus, a 2-fold increase in phosphorylated GSK3-β, and an increase in WNT3a secretion in the medium (Figures 4G–4J; quantification in Figure S6). Using GSEA, we confirmed that miR-600 OE compared to miR-600 KD transcriptomics experiments resulted in a downregulation of WNT target genes (Figure S6). Interestingly, tumors generated from PDX infected with miR-600 OE presented an absence of nuclear β-catenin staining, whereas 10% of the cells from PDX infected with the control vector presented a nuclear staining for β-catenin (Figure S6). Moreover, the inhibition of *SCD1* in miR-600 KD condition restored the basal β-catenin transactivator activity found in control cells (Figure 4K) and a downregulation of WNT target genes (Figure S6), further supporting a miR-600/SCD-1/WNT regulation axis. Due to the role of SCD1 in the production of OA, we measured the intracellular level of free OA following miR-600 modulation. Consistent with our other data, miR-600 OE decreased the intracellular level of free OA, whereas miR-600 KD induced a 2-fold increase (Figure S6). Because the role of SCD1 in the production of lipid-modified WNT proteins should not be restricted to the canonical WNT pathway, we also tested the effect of miR-600 modulation on the non-canonical WNT pathway. We used an ATF2 reporter assay to monitor the non-canonical WNT pathway and observed results similar to those obtained with the β-catenin reporter assay, suggesting an equivalent effect on both the canonical and non-canonical WNT pathways (Figure S6). Taken together, these results suggest that miR-600 acts as an intracellular bimodal regulator of WNT signaling through SCD1 regulation.

miR-600 Controls the WNT Signaling Regulatory Loop

WNT/β-catenin signaling activity is known to be maintained through a regulatory autocrine loop. We first evaluated the potential of miR-600 in regulating a loop involving secreted factors. We treated miR-600 OE cells with conditioned medium (CM) from miR-600 OE or KD cells (Figure 5A). As expected, CM from miR-600 OE cells did not modify the CSC proportion in

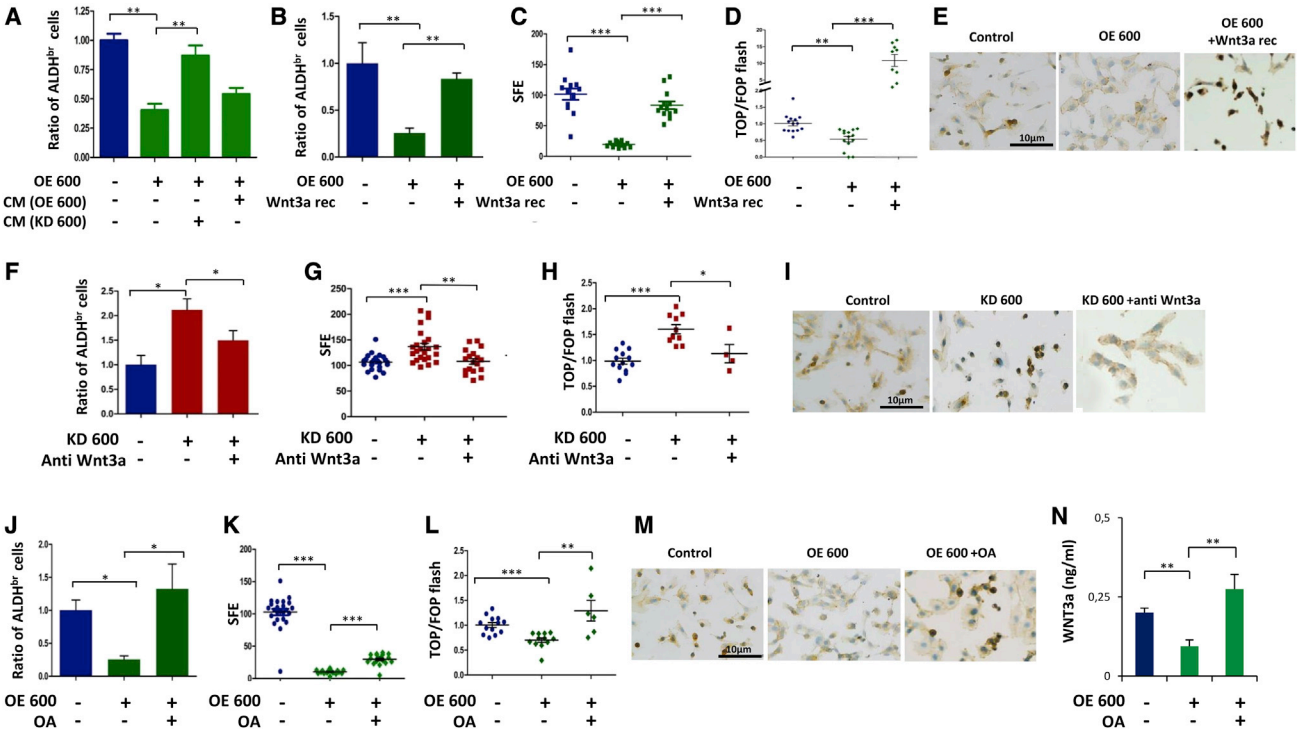

Figure 5. miR-600 Is Critical in Regulating the WNT Signaling Regulatory Autocrine Loop

(A) Evaluation of compensatory effects of conditioned medium (CM) from cells treated with miR-600 KD or OE.

(B–N) Evaluation of compensatory effects of WNT3A supplementation (B–E), WNT3A neutralizing antibody (F–I), and exogenous oleic acid (OA) (J–N) on the WNT signaling pathway in the bCSC population with miR-600 KD or OE. (B, F, and J) Evolution of the relative proportion of ALDH^{br} cell after the compensatory treatments. (C, G, and K) Bee swarm plots of the number of tumorspheres formed (SFE) after the compensatory treatments. (D, H, and L) Bee swarm plots of β-catenin transactivation measured by TOPflash after the compensatory treatments. (E, I, and M) Representative β-catenin immunostainings (brown staining) after the compensatory treatments. (N) Level of soluble WNT3A in the medium measured by ELISA assay after OA supplementation. In bee swarm plots, a dot corresponds to an individual experiment. Results are expressed as mean ± SD (*$p < 0.05$; **$p < 0.01$;***$p < 0.001$).

miR-600 OE cells, whereas CM from miR-600 KD cells restored the ALDH^{br} cell population, suggesting that miR-600 participates to the regulation of important secreted factors for CSC equilibrium. Next, we hypothesized that miR-600 toggles this regulatory loop by directly controlling the production of active WNT ligands secreted. According to this hypothesis, an extracellular WNT ligand should bypass miR-600 function. Thus, we evaluated the compensatory effect of exogenous WNT3A addition in the medium of miR-600 OE cells. WNT3A treatment indeed restored the ALDH^{br} cell population and the tumorsphere-formation efficiency (Figures 5B and 5C). The restoration of the CSC population was accompanied by an activation of the WNT/β-catenin signaling as shown by the increased β-catenin transcriptional activity and its nuclear accumulation (Figures 5D and 5E; quantification in Figure S6). Conversely, by inhibiting WNT/β-catenin signaling using a WNT3A neutralizing antibody, we suppressed the miR-600-KD-induced increase in CSCs (Figures 4F and 4G) and restored initial WNT/β-catenin signaling to the levels observed in control cells (Figures 4H and 4I; quantification in Figure S6). Finally, addition of exogenous OA to the culture medium rescued the miR-600-OE-induced effect: it restored the number of ALDH^{br} cells (Figure 5J), partially restored the tumorsphere-formation efficiency (Figure 5K), and reactivated WNT/β-catenin signaling and WNT3A secretion in the medium (Figures 5L–5N; quantification in Figure S6). These observations further support a model in which miR-600 drives a bimodal switch that balances bCSC-fate decisions by controlling the WNT/β-catenin regulatory autocrine loop (Figure 6). Interestingly, β-catenin silencing induced a decrease in endogenous miR-600 expression (Figure S6), suggesting that a negative feedback regulatory loop might be needed to maintain CSC proportions at steady state.

miR-600 Expression Is Associated with Prognosis in Breast Cancer Patients

To evaluate the clinical relevance of the above findings in human breast cancer, the expression of miR-600 was measured in 120 breast tumor samples using qRT-PCR. The expression of miR-600 was elevated in 28 patients (miR-600^{high} group), whereas the remaining 92 patients had miR-600 expression levels comparable to the normal breast epithelium (miR-600^{low} group). Interestingly, in our cell models with an ectopic overexpression of miR-600 (cell lines with miR-600 OE or PDXs with Lenti-miR-600 OE), the miR-600 expression level was comparable to the endogenous expression level observed in tumors from the miR-600^{high} group (Figure S7), which qualify our previous experiments as physiologically relevant. In patient samples, miR-600

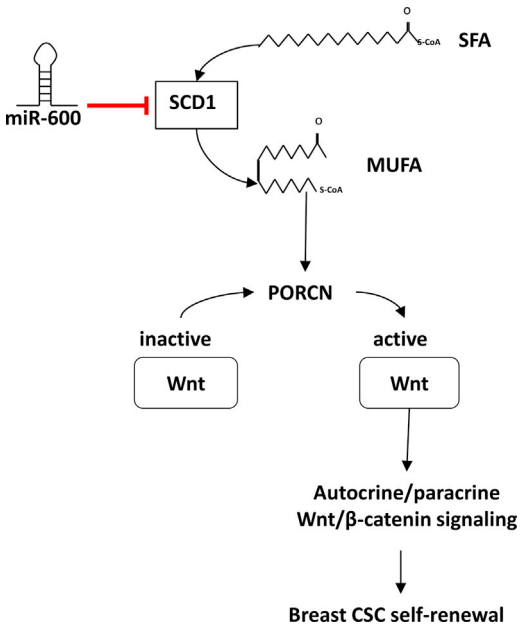

Figure 6. Simplified Model of bCSC Bimodal Regulation by the miR-600/SCD1/WNT Axis

miR-600 inhibits SCD1 to control bCSC-fate by regulating the sources of lipids needed to activate WNT.

expression was not associated with conventional histoclinical parameters (Table S4). miR-600^{high} tumors exhibited a lower β-catenin activation level with an absence of β-catenin nuclear staining, whereas 21% of miR-600^{low} tumors presented a nuclear localization of β-catenin ($p < 0.035$) (Figures 7A and 7B). Patients with miR-600^{high} tumors had a better overall survival (OS) than patients with miR-600^{low} tumors (5-year overall survival of 97% versus 81%, $p = 0.028$) (Figure 7C). These results suggest that miR-600 is a clinically relevant player in breast cancer tumorigenicity.

DISCUSSION

Delineating the intrinsic regulatory network that defines the CSC state is a prerequisite to develop more effective cancer therapies. This state is maintained by a transcriptional regulatory circuit that controls critical cellular processes, including self-renewal and differentiation. In this study, we have combined gain- and loss-of-function miRNome-wide screens and identified miR-600 as a bimodal switch regulator of bCSC fate. miR-600 KD resulted in an expansion of the phenotypic and functional bCSC compartment. Conversely, overexpression of miR-600 resulted in bCSC depletion and reduced tumorigenicity in xenograft experiments. Several miRNA switches have already been described as "fine-tuners" of stem cell fate. miR-126 governs the hematopoietic stem cell (HSC) pool size by controlling HSC cycle progression through regulation of the phosphatidylinositol 3-kinase (PI3K)/AKT/GSK3-β pathway (Lechman et al., 2012). In colon cancer, miR-34a regulates NOTCH signaling and acts as a CSC-fate determinant by altering the balance between self-renewal and differentiation (Bu et al., 2013). More recently, the concept of miRNA switches has been extended to human pluripotent stem cells (hPSCs) with the identification of several distinct miRNA switches that define hPSC-derived cell determination (Miki et al., 2015). It is conceivable that the concept of miRNA switches as stem cell-fate determinants could be generalized to a broader series of normal tissues and cancer types. In the future, the identification of these miRNAs will help decipher the regulatory circuits that control stem cell-fate decisions.

Beyond the identification of the miR-600 switch, our study established its underlying molecular mechanism. Neither the target genes of miR-600 nor its function was known. We identified SCD1 and MBD2 as two functional targets of mi-R600. The MBD proteins induce transcriptional silencing by blocking transcription or other protein factors from binding to DNA or by inducing chromatin remodeling through their binding partners. Interestingly, MBD2 has been shown to regulate pluripotency in human pluripotent stem cells (Wood and Zhou, 2016). Further investigation is needed to evaluate the potential of MBD2 in regulating bCSC fate. This study focused on the miR-600/SCD1 axis that controls bCSC fate through regulation of the WNT signaling pathway. Several studies have reported the prominent role of the WNT pathway in orchestrating CSC proliferation and differentiation in different solid tumors, including breast cancer (Ring et al., 2014). We previously demonstrated that GSK3-β is an essential crossing point in the regulation of the WNT-driven bCSC self-renewal. Indeed, dysregulation of the PTEN/PI3K/AKT pathway induces the expansion of the CSC pool by activation of the WNT/β-catenin pathway through the phosphorylation of GSK3-β (Korkaya et al., 2009). In the present study, we have identified a second essential crossing point where the miR-600/SCD1/PORCN pathway regulates WNT signaling to control bCSC fate. The production of a lipid-modified WNT protein appears to be a key step in the maintenance of the bCSC population. PORCN is known to be a non-redundant node for the regulation of global WNT signaling, because PORCN-null cells are incapable of autocrine WNT signaling (Proffitt and Virshup, 2012). Pharmacological inhibitors of PORCN demonstrated a strong potential in inhibiting WNT-dependent cancer (Proffitt et al., 2013; van de Wetering et al., 2015; Chen et al., 2009) and are presented as a new class of anti-CSC agents (Takebe et al., 2015). The role of SCD1 in WNT signaling has recently gained prominence as the provider of MUFAs to PORCN (Rios-Esteves and Resh, 2013). Interestingly, SCD1 is overexpressed in lung-cancer-initiating cells, and its inhibition selectively kills lung CSCs (Noto et al., 2013). Moreover, a high-throughput screen of a large chemical compound bank identified several SCD1 inhibitors as specific pluripotent cell inhibitors (Ben-David et al., 2013). Our findings are consistent with these reports and provide new insights into the role of WNT in bCSC-fate choices by uncovering a regulatory circuit where miR-600 acts as the master determinant of a key WNT signaling crossing point. Beside its role in WNT signaling, SCD1 has been described as an important coordinator of the lipid biosynthesis and energy production (Igal, 2010). Recent studies have described a specific metabolic activity in the CSC population as a crucial element in the maintenance of CSC properties (for review, see Deshmukh et al., 2016). Based on our results, SCD1 may be considered an important regulator of the CSC's metabolic switch.

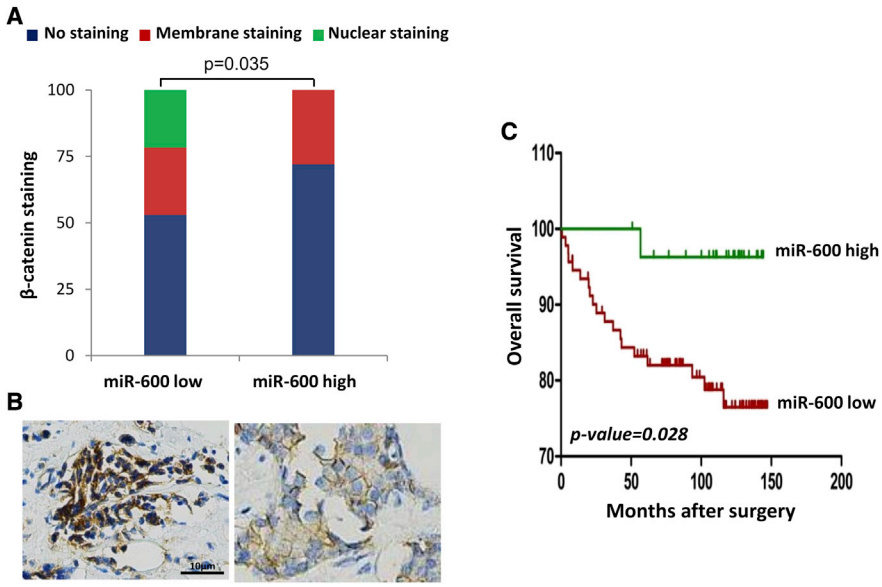

Figure 7. Clinical Association between miR-600 Expression and Breast Cancer Prognosis

(A) Stacked bar chart of the relative β-catenin immunostaining proportions (red, membrane; green, nucleus; and blue, no staining) in breast tumor samples. Patient samples were grouped according to their miR-600 expression level. miR-600^{high} tumors exhibit an absence of β-catenin nuclear staining, whereas 21% of miR-600^{low} tumors present a nuclear localization of β-catenin (chi-square test, $p < 0.035$).

(B) Representative tumor sample sections with β-catenin immunostaining (in brown). Left: miR-600^{high} tumor with cytoplasmic and membrane β-catenin staining. Right: miR-600^{low} tumor with nuclear β-catenin staining.

(C) Kaplan-Meier overall survival curve according to miR-600 expression levels in tumors. There is an association between a high level of miR-600 expression and better overall survival (log-rank test, $p = 0.028$).

This report links a miRNA to the regulation of bCSC fate. The clinical relevance of these observations was shown in patient tumor samples where miR-600 overexpression was associated with an absence of β-catenin activation and a better prognosis. Given the close relationship between the clinical behavior and the CSC content of a tumor (Kreso and Dick, 2014), our observation opens an avenue to develop new therapeutic strategies targeting the miR-600/SCD1/PORCN axis. Moreover, our findings indicate that miR-600 can be added to the list of feedback loop regulators controlling WNT signaling. Finding ways to block these loops is essential in WNT targeting. Besides SCD1 and PORCN inhibition, nanovectorized miR-600 agonist (pre-miRNA) may potentially represent an efficient anti-CSC therapeutic approach. Finally, considering the role of WNT signaling in breast tumor progression, future studies should examine whether miR-600 deregulation contributes to breast tumor genesis.

EXPERIMENTAL PROCEDURES

Ethics Statement

Samples of human origin and the associated data were obtained from the Institut Paoli-Calmettes/Cancer Research Center of Marseille (IPC/CRCM) Tumor Bank, which operates under authorization number AC-2013-1905 granted by the French Ministry of Research (“Ministère de la Recherche et de l’Enseignement Supérieur”). Prior to scientific use of samples and data, patients were appropriately informed and filed a written consent, in compliance with French and European regulations. Animal studies were approved by the INSERM office for Laboratory Animal Medicine (Marseille, France).

Cell Culture

Three breast cancer cell lines from three distinct molecular subtypes (SUM149/Basal, SUM159/Mesenchymal and S68/Luminal) were used in this study. All BCLs were grown in standard medium as previously described (Charafe-Jauffret et al., 2013). For Wnt3a antibody rescue, miR-600 KD cells were treated with Wnt3a-neutralizing antibody (R&D Systems) directly added into the medium at 5 μg/mL. Similarly, rescue experiments were performed in miR-600 OE cells using Wnt3a recombinant proteins (0.1 μg/mL) or 100μM of OA-BSA (Sigma). Conditioned medium (CM) from cells maintained 3 days in culture was prepared using ultracentrifugal filters (Amicon, 10 kDa). 12 mL CM was concentrated down to 250 μL before performing rescue experiments. Cell culture conditions for tumorsphere formation are described in Supplemental Experimental Procedures.

Breast Cancer Samples

Breast cancer samples were collected from a cohort of 120 consecutive patients with invasive breast cancers who underwent surgical biopsies or initial surgery at the Institut Paoli-Calmettes (Marseille, France) during the year 2002. Histoclinical characteristics were established for the 120 breast cancer samples as described in Table S4. A TMA containing 120 breast cancer cores from the tumor cohort was constructed and used to evaluate β-catenin protein expression and localization as described in Supplemental Experimental Procedures.

Cell Transfection and Miniaturized ALDEFLUOR Assay

We performed two concurrent miRNome-wide screenings in SUM159 cell line using miRNA OE and KD libraries. KD library contained LNA miRNA inhibitors with normalized Tm (miRCURY LNA human miRNA Inhibitor Library, 1023 LNA probes, catalog number 190102-00, Exiqon), designed to target and neutralize 954 human miRNAs listed in miRBase v.12. The OE library contained pre-miR hairpins (1,090 human miRNA precursor library, catalog number AM17102, Ambion) designed to mimic 1,240 human miRNAs listed in miRBase v.15.0.

For screening purpose, an automated reverse transfection protocol of LNA probes or pre-miRs was developed as described in Supplemental Experimental Procedures.

Cell Proliferation Rate

Cells were transfected with siRNAs, pre-miRs or LNAs in 96-well format as described earlier. 24, 48, and 72 hr post-transfection, cells were fixed in paraformaldehyde 4% (w/v, Sigma), and nucleic acids were stained overnight with Hoechst 33342 (5 μg/mL). After replacement of paraformaldehyde (PFA) by PBS, plates were imaged using an Operetta High Content Imaging device (10× magnification, nine fields per well). Images acquired in the blue channel were segmented to detect nuclei, and results were expressed as percentage of cells relative to the respective negative control (scrambled siRNA or LNA, value set to 1).

Apoptotic Rate

Cells were analyzed for phosphatidylserine exposure and cell membrane rupture by an Annexin-V fluorescein isothiocyanate (FITC)/propidium iodide (PI) double-staining method as described by the manufacturer (Santa Cruz Biotechnology). Cells cultured in 96-well format were collected 72 hr post-lipofection and subjected to the analysis. A minimum of 10,000 cells per condition were analyzed by cytometry (Guava Easycyte HT, Merck Millipore). Annexin-V- and PI-negative cells were considered as viable, while Annexin-V-positive and PI-negative cells were considered as early apoptotic cells and double-positive cells were considered as cells in end-stage apoptosis.

ELISA Assay

To measure the level of soluble WNT3a secreted in the culture medium of breast cancer cell lines, we utilized a human WNT3a ELISA kit from MyBiosource as described by the manufacturer. Absorbance was read on a spectro-photometer using 450 nm as the primary wavelength. Each measurement was done in quadruplicate. For each replicate, the total cell number was evaluated and used to normalize the level of soluble WNT3a detected.

miRNA Extraction and Quantitative Real-Time PCR

MicroRNAs were extracted from cultured cell lines and PDXs using miReasy micro kit (QIAGEN) and from paraffin-embedded normal and malignant breast tissues using RecoverAll Total Nucleic Acid Isolation Kit (Ambion). 500 ng RNA was reverse transcribed in accordance with manufacturer's instruction (Superscript II reverse transcriptase, Invitrogen). miRNA expression levels were quantified using TaqMan probes as described in Supplemental Experimental Procedures.

Animal Models

Two established primary human breast cancer xenografts were generated from two different patients (CRCM494 and CRCM168) (Charafe-Jauffret et al., 2013). Tumors were dissociated into single cells and infected overnight at 37°C with smart choice human lentiviral has-miR600 (GE Healthcare), hsa-miR600-sponge lentivirus (Creative Biogene), or DsRed control lentivirus in the presence of Polybrene (10 μg/mL). Infected cells were then cultured in non-adherent conditions for 3 days, filtered, and dissociated using trypsin 0.05% (w/v, Gibco), and DsRed-positive cells were sorted using an ARIA III cytometer (Becton Dickinson). For the limiting dilution assay, sorted cells were suspended in 100 μL of a mixture of FBS/Matrigel (v/v) (Invitrogen) and injected orthotopically in the humanized cleared fat pad of non-obese diabetic/severe combined immunodeficiency (NOD/SCID) mice. To avoid tumor necrosis, and in compliance with regulations for use of vertebrate animals in research, animals were euthanized when the tumors reached ~1 cm in the largest diameter. A portion of each injected fat pad was fixed in formalin and embedded in paraffin for histological analysis.

Gene Expression Profiling

RNA expression data were generated using Affymetrix ST2.0 oligonucleotide microarrays as described in Supplemental Experimental Procedures.

SCD1 3′ UTR Reporter Assay

To validate miR-600's direct interaction with SCD1, we developed a reporter assay using two plasmids (LightSwitch Luciferase vector) with luciferase expression under control of either the wild-type SCD1 3′ UTR (SCD1-WT) or the SCD1 3′ UTR with mutations brought into the seed sequence of miR600 site (SCD1 mutant). We also used a Cypridina TK Control Vector (Active Motif) as reporter of transfection efficiency. 24 hr post-transfection, luciferase expression was revealed using LightSwitch Dual assay kit (Active Motif) according to the manufacturer's instructions. Data were first normalized to the Cypridina TK control vector and then expressed as the SCD1-WT/SCD1 mutant ratio.

Wnt Pathways Reporter Assays

Canonical Wnt/β-catenin signaling activation was evaluated using a β-catenin reporter assay (TOP flash assay), and for the non-canonical WNT signal, we used an ATF2 reporter assay (QIAGEN). Similar transfection and culture conditions were used for both assays as described in Supplemental Experimental Procedures.

Free Fatty Acid Methyl Ester Analysis

Lipids corresponding to 1.5 million cells were extracted in dichloromethane/methanol/water (2.5:2.5:2.1, v/v/v), in the presence of the internal standard heptadecanoate acid. The lipid extracts were directly methylated in boron trifluoride methanol solution 14% (w/v, Sigma) and heptane at real time (RT) for 10 min. After addition of water to the crude, free fatty acid methyl esters (FAMEs) were extracted with heptane, dried by evaporation and dissolved in ethyl acetate. FAMEs were analyzed by gas-liquid chromatography on a Clarus 600 system (Perkin Elmer) using fused silica capillary column (30 m × 0.32 mm i.d, 0.25 μm, Famewax RESTEK 0.5). The injector and the detector were heated at 225°C and 245°C respectively.

Statistical Analysis

GraphPad Prism 5.0 was used for data analysis and imaging. Results are presented as the mean ± SD for at least three repeated independent experiments. To investigate associations among variables, univariate analysis were performed using non-parametric Wilcoxon rank sum test, chi-square test or Fisher's exact test when appropriate. Extreme LDA (http://bioinf.wehi.edu.au/software/elda/) was used to evaluate bCSC frequency. GSEA significance cutoffs were FDR < 0.25, $p < 0.05$. The Kaplan-Meier method was used to establish survival curves, and curves were compared with the log-rank test. In all cases, a p value < 0.05 was considered as statistically significant.

ACCESSION NUMBERS

The accession number for the gene expression profile reported in this paper is ArrayExpress: E-MTAB-5393.

SUPPLEMENTAL INFORMATION

Supplemental Information includes Supplemental Experimental Procedures, seven figures, and four tables and can be found with this article online at http://dx.doi.org/10.1016/j.celrep.2017.02.016.

AUTHOR CONTRIBUTIONS

D.B., E.C.-J., and C.G. designed research studies; R.E.H., G.P., O.C., J.W., P.F., and A.G. conducted experiments and acquired data; R.E.H., G.P., R.B., L.G., C.R., P.F., B.M., P.B., F.B., G.B., A.H.-B., E.C.-J., D.B., and C.G. analyzed data; G.P., B.M., P.B., and A.H.-B. provided reagents; and R.E.H., E.C.-J., and C.G. wrote the manuscript.

ACKNOWLEDGMENTS

We express our gratitude to the Fondation ARC for supporting the acquisition of our cell sorter. Thanks are due to the MetaToul-Lipidomique Core Facility (I2MC, INSERM 1048, Toulouse, France), MetaboHUB-ANR-11-INBS-0010, the CRCM flow cytometry and animal core facilities. We thank Gisèle Froment, Didier Nègre, and Caroline Costa from the lentivectors production facility/SFR BioSciences Gerland-Lyon Sud (UMS3444/US8). This study was supported by

INSERM, Institut Paoli-Calmettes, INCa (INCa_5911), SIRIC Marseille (INCa-DGOS-INSERM 6038), GEFLUC, and the Ligue National Contre le Cancer (Label DB). R.H. was supported by a fellowship from the French Ministry of Research.

Received: June 22, 2016
Revised: December 15, 2016
Accepted: February 2, 2017
Published: February 28, 2017

REFERENCES

Ben-David, U., Gan, Q.F., Golan-Lev, T., Arora, P., Yanuka, O., Oren, Y.S., Leikin-Frenkel, A., Graf, M., Garippa, R., Boehringer, M., et al. (2013). Selective elimination of human pluripotent stem cells by an oleate synthesis inhibitor discovered in a high-throughput screen. Cell Stem Cell *12*, 167–179.

Bhajun, R., Guyon, L., Pitaval, A., Sulpice, E., Combe, S., Obeid, P., Haguet, V., Ghorbel, I., Lajaunie, C., and Gidrol, X. (2015). A statistically inferred microRNA network identifies breast cancer target miR-940 as an actin cytoskeleton regulator. Sci. Rep. *5*, 8336.

Bu, P., Chen, K.Y., Chen, J.H., Wang, L., Walters, J., Shin, Y.J., Goerger, J.P., Sun, J., Witherspoon, M., Rakhilin, N., et al. (2013). A microRNA miR-34a-regulated bimodal switch targets Notch in colon cancer stem cells. Cell Stem Cell *12*, 602–615.

Cai, J., Guan, H., Fang, L., Yang, Y., Zhu, X., Yuan, J., Wu, J., and Li, M. (2013). MicroRNA-374a activates Wnt/β-catenin signaling to promote breast cancer metastasis. J. Clin. Invest. *123*, 566–579.

Charafe-Jauffret, E., Ginestier, C., Iovino, F., Wicinski, J., Cervera, N., Finetti, P., Hur, M.H., Diebel, M.E., Monville, F., Dutcher, J., et al. (2009). Breast cancer cell lines contain functional cancer stem cells with metastatic capacity and a distinct molecular signature. Cancer Res. *69*, 1302–1313.

Charafe-Jauffret, E., Ginestier, C., Bertucci, F., Cabaud, O., Wicinski, J., Finetti, P., Josselin, E., Adelaide, J., Nguyen, T.T., Monville, F., et al. (2013). ALDH1-positive cancer stem cells predict engraftment of primary breast tumors and are governed by a common stem cell program. Cancer Res. *73*, 7290–7300.

Chen, B., Dodge, M.E., Tang, W., Lu, J., Ma, Z., Fan, C.W., Wei, S., Hao, W., Kilgore, J., Williams, N.S., et al. (2009). Small molecule-mediated disruption of Wnt-dependent signaling in tissue regeneration and cancer. Nat. Chem. Biol. *5*, 100–107.

Cioffi, M., Trabulo, S.M., Sanchez-Ripoll, Y., Miranda-Lorenzo, I., Lonardo, E., Dorado, J., Reis Vieira, C., Ramirez, J.C., Hidalgo, M., Aicher, A., et al. (2015). The miR-17-92 cluster counteracts quiescence and chemoresistance in a distinct subpopulation of pancreatic cancer stem cells. Gut *64*, 1936–1948.

Deshmukh, A., Deshpande, K., Arfuso, F., Newsholme, P., and Dharmarajan, A. (2016). Cancer stem cell metabolism: a potential target for cancer therapy. Mol. Cancer *15*, 69–79.

Djuranovic, S., Nahvi, A., and Green, R. (2011). A parsimonious model for gene regulation by miRNAs. Science *331*, 550–553.

Garcia, D.M., Baek, D., Shin, C., Bell, G.W., Grimson, A., and Bartel, D.P. (2011). Weak seed-pairing stability and high target-site abundance decrease the proficiency of lsy-6 and other microRNAs. Nat. Struct. Mol. Biol. *18*, 1139–1146.

Garofalo, M., and Croce, C.M. (2015). Role of microRNAs in maintaining cancer stem cells. Adv. Drug Deliv. Rev. *81*, 53–61.

Ginestier, C., Hur, M.H., Charafe-Jauffret, E., Monville, F., Dutcher, J., Brown, M., Jacquemier, J., Viens, P., Kleer, C.G., Liu, S., et al. (2007). ALDH1 is a marker of normal and malignant human mammary stem cells and a predictor of poor clinical outcome. Cell Stem Cell *1*, 555–567.

Hwang, W.L., Jiang, J.K., Yang, S.H., Huang, T.S., Lan, H.Y., Teng, H.W., Yang, C.Y., Tsai, Y.P., Lin, C.H., Wang, H.W., and Yang, M.H. (2014). MicroRNA-146a directs the symmetric division of Snail-dominant colorectal cancer stem cells. Nat. Cell Biol. *16*, 268–280.

Igal, R.A. (2010). Stearoyl-CoA desaturase-1: a novel key player in the mechanisms of cell proliferation, programmed cell death and transformation to cancer. Carcinogenesis *31*, 1509–1515.

Korkaya, H., Paulson, A., Charafe-Jauffret, E., Ginestier, C., Brown, M., Dutcher, J., Clouthier, S.G., and Wicha, M.S. (2009). Regulation of mammary stem/progenitor cells by PTEN/Akt/beta-catenin signaling. PLoS Biol. *7*, e1000121.

Kreso, A., and Dick, J.E. (2014). Evolution of the cancer stem cell model. Cell Stem Cell *14*, 275–291.

Le Brigand, K., Robbe-Sermesant, K., Mari, B., and Barbry, P. (2010). MiRonTop: mining microRNAs targets across large scale gene expression studies. Bioinformatics *26*, 3131–3132.

Lechman, E.R., Gentner, B., van Galen, P., Giustacchini, A., Saini, M., Boccalatte, F.E., Hiramatsu, H., Restuccia, U., Bachi, A., Voisin, V., et al. (2012). Attenuation of miR-126 activity expands HSC in vivo without exhaustion. Cell Stem Cell *11*, 799–811.

Liu, S., and Wicha, M.S. (2010). Targeting breast cancer stem cells. J. Clin. Oncol. *28*, 4006–4012.

Liu, C., Kelnar, K., Liu, B., Chen, X., Calhoun-Davis, T., Li, H., Patrawala, L., Yan, H., Jeter, C., Honorio, S., et al. (2011). The microRNA miR-34a inhibits prostate cancer stem cells and metastasis by directly repressing CD44. Nat. Med. *17*, 211–215.

Liu, S., Clouthier, S.G., and Wicha, M.S. (2012a). Role of microRNAs in the regulation of breast cancer stem cells. J. Mammary Gland Biol. Neoplasia *17*, 15–21.

Liu, S., Patel, S.H., Ginestier, C., Ibarra, I., Martin-Trevino, R., Bai, S., McDermott, S.P., Shang, L., Ke, J., Ou, S.J., et al. (2012b). MicroRNA93 regulates proliferation and differentiation of normal and malignant breast stem cells. PLoS Genet. *8*, e1002751.

Ma, S., Tang, K.H., Chan, Y.P., Lee, T.K., Kwan, P.S., Castilho, A., Ng, I., Man, K., Wong, N., To, K.F., et al. (2010). miR-130b promotes CD133(+) liver tumor-initiating cell growth and self-renewal via tumor protein 53-induced nuclear protein 1. Cell Stem Cell *7*, 694–707.

Miki, K., Endo, K., Takahashi, S., Funakoshi, S., Takei, I., Katayama, S., Toyoda, T., Kotaka, M., Takaki, T., Umeda, M., et al. (2015). Efficient Detection and Purification of Cell Populations Using Synthetic MicroRNA Switches. Cell Stem Cell *16*, 699–711.

Noto, A., Raffa, S., De Vitis, C., Roscilli, G., Malpicci, D., Coluccia, P., Di Napoli, A., Ricci, A., Giovagnoli, M.R., Aurisicchio, L., et al. (2013). Stearoyl-CoA desaturase-1 is a key factor for lung cancer-initiating cells. Cell Death Dis. *4*, e947.

Polesskaya, A., Degerny, C., Pinna, G., Maury, Y., Kratassiouk, G., Mouly, V., Morozova, N., Kropp, J., Frandsen, N., and Harel-Bellan, A. (2013). Genome-wide exploration of miRNA function in mammalian muscle cell differentiation. PLoS ONE *8*, e71927.

Polytarchou, C., Iliopoulos, D., and Struhl, K. (2012). An integrated transcriptional regulatory circuit that reinforces the breast cancer stem cell state. Proc. Natl. Acad. Sci. USA *109*, 14470–14475.

Proffitt, K.D., and Virshup, D.M. (2012). Precise regulation of porcupine activity is required for physiological Wnt signaling. J. Biol. Chem. *287*, 34167–34178.

Proffitt, K.D., Madan, B., Ke, Z., Pendharkar, V., Ding, L., Lee, M.A., Hannoush, R.N., and Virshup, D.M. (2013). Pharmacological inhibition of the Wnt acyltransferase PORCN prevents growth of WNT-driven mammary cancer. Cancer Res. *73*, 502–507.

Ring, A., Kim, Y.M., and Kahn, M. (2014). Wnt/catenin signaling in adult stem cell physiology and disease. Stem Cell Rev. *10*, 512–525.

Rios-Esteves, J., and Resh, M.D. (2013). Stearoyl CoA desaturase is required to produce active, lipid-modified Wnt proteins. Cell Rep. *4*, 1072–1081.

Shannon, P., Markiel, A., Ozier, O., Baliga, N.S., Wang, J.T., Ramage, D., Amin, N., Schwikowski, B., and Ideker, T. (2003). Cytoscape: a software environment for integrated models of biomolecular interaction networks. Genome Res. *13*, 2498–2504.

Shimono, Y., Zabala, M., Cho, R.W., Lobo, N., Dalerba, P., Qian, D., Diehn, M., Liu, H., Panula, S.P., Chiao, E., et al. (2009). Downregulation of miRNA-200c links breast cancer stem cells with normal stem cells. Cell *138*, 592–603.

Song, S.J., Ito, K., Ala, U., Kats, L., Webster, K., Sun, S.M., Jongen-Lavrencic, M., Manova-Todorova, K., Teruya-Feldstein, J., Avigan, D.E., et al. (2013). The oncogenic microRNA miR-22 targets the TET2 tumor suppressor to promote hematopoietic stem cell self-renewal and transformation. Cell Stem Cell *13*, 87–101.

Srivastava, A.K., Han, C., Zhao, R., Cui, T., Dai, Y., Mao, C., Zhao, W., Zhang, X., Yu, J., and Wang, Q.E. (2015). Enhanced expression of DNA polymerase eta contributes to cisplatin resistance of ovarian cancer stem cells. Proc. Natl. Acad. Sci. USA *112*, 4411–4416.

Takebe, N., Miele, L., Harris, P.J., Jeong, W., Bando, H., Kahn, M., Yang, S.X., and Ivy, S.P. (2015). Targeting Notch, Hedgehog, and Wnt pathways in cancer stem cells: clinical update. Nat. Rev. Clin. Oncol. *12*, 445–464.

Taube, J.H., Malouf, G.G., Lu, E., Sphyris, N., Vijay, V., Ramachandran, P.P., Ueno, K.R., Gaur, S., Nicoloso, M.S., Rossi, S., et al. (2013). Epigenetic silencing of microRNA-203 is required for EMT and cancer stem cell properties. Sci. Rep. *3*, 2687.

van de Wetering, M., Francies, H.E., Francis, J.M., Bounova, G., Iorio, F., Pronk, A., van Houdt, W., van Gorp, J., Taylor-Weiner, A., Kester, L., et al. (2015). Prospective derivation of a living organoid biobank of colorectal cancer patients. Cell *161*, 933–945.

Visvader, J.E., and Lindeman, G.J. (2012). Cancer stem cells: current status and evolving complexities. Cell Stem Cell *10*, 717–728.

Wang, H., Sun, T., Hu, J., Zhang, R., Rao, Y., Wang, S., Chen, R., McLendon, R.E., Friedman, A.H., Keir, S.T., et al. (2014). miR-33a promotes glioma-initiating cell self-renewal via PKA and NOTCH pathways. J. Clin. Invest. *124*, 4489–4502.

Wood, K.H., and Zhou, Z. (2016). Emerging molecular and biological functions of MBD2, a reader of DNA methylation. Front. Genet. *7*, 93.

Yu, F., Yao, H., Zhu, P., Zhang, X., Pan, Q., Gong, C., Huang, Y., Hu, X., Su, F., Lieberman, J., and Song, E. (2007). let-7 regulates self renewal and tumorigenicity of breast cancer cells. Cell *131*, 1109–1123.